Radar remote sensing for damage assessment: case study on L'Aquila, Italy, 6th April 2009 earthquake.

Fabio Dell'Acqua, Diego Polli

Dipartimento di Elettronica, Università di Pavia, via Ferrata, 1 I-27100 Pavia
{name.surname}@unipv.it

KEY WORDS: satellite remote sensing, earthquake, rapid mapping

ABSTRACT:

Destructive earthquakes, as much as other natural disasters, represent a challenge for Earth Observation (EO) systems to demonstrate their usefulness in supporting intervention and relief actions. The use of EO data in a disaster context has been widely investigated by many actors, but only recently the developed methods seem to have reached near to the operational use. In this paper a case study on the 6th April 2009 earthquake event, which stroke L'Aquila, Italy, is considered. In particular, the use of new-generation satellite Very High Resolution (VHR) radar data such as those provided by the COSMO/SkyMed constellation opens new opportunities. Such data may be profitably used for damage assessment and for detection of relevant objects on the disaster site. Satisfying results may be achieved if the damage is assessed at a block level, somehow averaging the unreliable -due to speckle noise- results of pixel-wise comparing pre-and post-event images. Though, pre-post event pairs have to be available, which may not be always the case for new generation, very high resolution systems like COSMO/SkyMed, especially when operated in spotlight mode. In this paper a preliminary study is described which investigates possible damage signatures in the post-event image alone, starting from texture measures and possibly integrating ancillary information like urban block partition and seismic vulnerability. In addition to such investigation, a detector of anomalous scatterers is also presented as a tool to support inspection of potentially dangerous structures in the observed area. The paper will illustrate and discuss the results and provide some clues for an operational use of the developed methods.

I. Introduction

When a strong and destructive event take place, an early response is very important to support and to manage the rescue activities. In this framework, satellite remote sensing can supply a useful instrument to help the decision chain of the civil protection authorities [1]. Thanks to the increasing interest and the great efforts by the scientific community mapping the damage of buildings and infrastructures using satellite data, is becoming a valuable and more reliable tool.

New generation satellite sensors, both optical and radar, can reach sub-meter spatial resolution, this new technology can be useful for damage mapping purpose.

In literature is possible to find several methods that exploit in different way the information carried by radar signal. For example in [2]-[5] has been created an index related to the damage level, combining SAR image intensity changes and the related correlation coefficient. Is also possible to compare SAR backscattering changes and signal phase changes respect to the damage occurred in a seismic event [6]. In [7] Ito et al. studied sensors working at different frequencies (L- and C- band) to derive change indicators. Comparing pre- and post-event backscattering data is a method to detect strong modification as shown in [8].

In the field of optical sensors, VHR images allow to detect damage at single building scale, but unfortunately this kind of data are affected by problems such as presence of shadows and their variation due to the sun illumination and geometric distortions. For this reason the most used techniques require visual inspection and interpretation [9], [10]. In [11] is presented a method based on the analysis of the edges in VHR data and in [12] is proposed a technique for the damage classification.

More generally, in literature are available many papers that show automatic change-detection algorithms exploiting both optical [13], [14] and SAR images [15], including multitemporal ones [16].

II. L'Aquila April 6th, 2009, Earthquake: From acquisition request to product delivery

The European Centre for Training and Research on Earthquake Engineering (EUCENTRE) is connected with the Italian Civil Protection Department (DPC), one of its founders, which is also the GMES Focal Point for Italy. Since the DPC is entitled to access COSMO/SkyMed imagery in emergency and it was obviously activated, the research centre could obtain SAR images over the affected areas soon after the earthquake took place.

The COSMO/SkyMed images were first delivered through the Internet by the Italian Space Agency (ASI) to the DPC, which then redistributed the same data to its related research centers via the same mechanism.

Image	N° satellite	Off nadir angle	Acquisition date	Acquisition hour
2454	SAR-1	50.57°	05/04/09	05:24.45
2524	SAR-1	50.57°	16/02/09	05:25.20
5457	SAR-3	19.07°	22/03/09	04:54.51
2450	SAR-3	50.57°	14/04/09	05:24.38
2451	SAR-2	50.50°	13/04/09	05:24.44
5445	SAR-3	19.07°	07/04/09	05:54.39

Table 1 : Data set information

After image delivery, a research work started in parallel to their operational processing.

III. Damage Assessment Research

Investigations on possible, simple signatures of the damage level from a post-event image alone were made and assessed against a corresponding pre-event image.

As all radar images, even COSMO/SkyMed ones are afflicted by speckle noise. So the first step is reduce this problem, to do this the Lee filter is performed on the whole image. Consequentially another filter is applied, based on the image histogram, is applied to remove this issue more deeply.

Next, analysis of the image histogram helps setting parameters for the subsequent thresholding and morphological processing of the reflectance map to find clusters of strongly reflective pixels likely to be associated with isolated, man-made structures. The resulting map, output in the form of a cloud of points in a GIS layer, supports the discovery of rural, man-made structure not found on the maps which may be in danger of collapse and should be inspected as soon as possible. The product is however still under development, and details will be explained in future papers once a consolidated procedure has been set up.

A. Damage assessment at block level

It is commonly acknowledged that due to speckle effects, single-pixel classification of SAR images leads to unsatisfactory results, and damage assessment is no exception. Satisfying results may be achieved at a block level aggregation, somehow averaging the unreliable results of pixel-wise comparing pre-and post-event images [1] due to speckle noise [19]. The bottleneck is availability of pre-post event pairs, far from being guaranteed for new generation, very high resolution systems like COSMO/SkyMed, especially when operated in spotlight mode. A preliminary study was thus initiated to investigate possible damage signatures in the post-event image alone. Visual inspection of the image allowed partitioning the urban area into 58 blocks output to a GIS layer (Fig. 1); the average block size is 0.1176 km^2 (with single polygons ranging from 0.0146 to 0.698) every polygon in the city centre covering around 100 buildings.

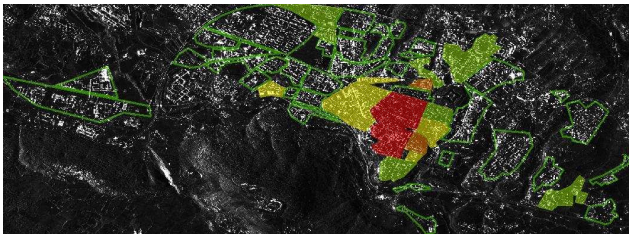

Figure 1 : Urban blocks on city layer. Damage level is colour coded (transparent = no damage; red = heaviest damage)

Once tuned, it is planned to use the procedure in [1] on areas where a GIS is not available. Each block was then compared with a layer containing footprints of severely damaged buildings visually extracted from post-event aerial images acquired by the Italian Air Force and kindly provided by the DPC. Such image allowed assigning a "Damaged Area Ratio" (DAR) to each block in the first layer:

$$DAR_j = \frac{\sum_i d_{ij} \cdot A_{ij}^B}{A_j^P} \qquad (1)$$

where:

- DAR_j is the DAR value on *j*-th GIS polygon
- d_{ij} is the "damage flag" (with values 0 or 1) indicating whether building *i* in polygon *j* was damaged by the earthquake
- A^B_{ij} is the footprint area of the *i*-th building in *j*-th polygon
- A^P_j is the total area of the *j*-th polygon

In the case at hand, DAR values ranged from zero to 46.4%, with an average value of 3.99% overall, rising to 11.02% if the average is computed only on the 21 blocks with DAR>0.

Several texture measures were then extracted at different window sizes from the geocoded COSMO/SkyMed image. Just to give a flavor of the features involved, average values of "variance" texture are around 10^7, ranging from minima on the order of 10^3 to maxima reaching 10^{12}. This wide variability probably reflects the strong speckle noise found in the image, still it apparently does not prevent significant correlations to emerge.

Texture measures were averaged over every one of the 58 blocks; $AT_j^{texturetype}$ indicates the "*texturetype*" texture measure averaged over pixels in j-*th* block. Correlations were then computed between DAR*j* and $AT_j^{texturetype}$ for *j*=1..58, over different texture measures and window sizes.

Correlation levels (see table I) are generally quite low, with absolute values below 0.1, except for variance, featuring correlations as high as 0.258.

	7x7	13x13	17x17	21x21
Data Range	-0.040	-0.055	-0.064	-0.072
Mean	-0.007	-0.004	-0.003	-0.002
Variance	-0.087	-0.086	-0.085	-0.084
Entropy	-0.023	-0.098	-0.088	-0.063

Table 2 : image 5445, correlation values occurrence texture

	21x21 (3;3)	21x21 (11;11)	51x51(21;21)
Mean	0.502	0.502	0.508
Variance	0.631	0.631	0.584
Homogeneity	-0.385	-0.386	-0.386
Contrast	0.627	0.603	0.567
Dissimilarity	0.599	0.579	0.549
Entropy	0.357	0.345	0.363
Second Moment	-0.211	-0.241	-0.226
Correlation	0.115	0.151	0.155

Table 3 : image 5445, correlation values co-occurrence texture

	7x7	13x13	17x17	21x21
Data Range	-0.037	-0.004	0.012	0.025
Mean	-0.099	-0.098	-0.098	-0.098
Variance	0.258	0.250	0.247	0.246
Entropy	-0.049	-0.026	-0.023	-0.031

Table 4 : image 2451, correlation values occurrence texture

	21x21 (3;3)	21x21 (11;11)	51x51(21;21)
Mean	-0.217	-0.217	-0.217
Variance	-0.103	-0.103	-0.128
Homogeneity	0.218	0.188	0.229
Contrast	-0.109	-0.128	-0.147
Dissimilarity	-0.095	-0.112	-0.133
Entropy	-0.178	-0.149	-0.172
Second Moment	0.181	0.168	0.254
Correlation	0.344	0.313	0.174

Table 5 : image 2451, correlation values co-occurrence texture

	7x7	13x13	17x17	21x21
Data Range	-0.095	-0.081	-0.072	-0.063
Mean	-0.135	-0.136	-0.136	-0.137
Variance	0.143	0.140	0.138	0.137
Entropy	-0.129	-0.172	-0.177	-0.163

Table 6 : image 2450, correlation values occurrence texture

	21x21 (3;3)	21x21 (11;11)	51x51(21;21)
Mean	-0.222	-0.222	-0.221
Variance	-0.115	-0.115	-0.142
Homogeneity	0.241	0.178	0.198
Contrast	-0.129	-0.137	-0.155
Dissimilarity	-0.120	-0.125	-0.143
Entropy	-0.190	-0.160	-0.167
Second Moment	0.209	0.193	0.225
Correlation	0.334	0.321	0.157

Table 7 : image 2450, correlation values co-occurrence texture

This result is however biased towards zero by at least two factors:

1. a large number of blocks (38 out of 58, around 65%) report no visible damage, and thus were labeled with zero, whilst a series of accidental factors connected with acquisition, cause the texture value to change among such blocks. This drags down the overall correlation.
2. The definition of DAR leads to a very precise and resolved numerical value for the damage level, while texture measures are structurally incapable to catch up with small fractions of damaged buildings. This, again, drags down the correlation value, but it does not necessarily mean that texture measures are useless in damage evaluation.

Far deeper investigations are required to cope with this latter issue, while to rule out the first bias factor a simple method is applicable, consisting of computing correlation on damaged blocks only. Results are reported in Table 8-13.

	7x7	13x13	17x17	21x21
Data Range	-0.087	-0.128	-0.149	-0.166
Mean	-0.004	0.008	0.012	0.015
Variance	-0.184	-0.186	-0.187	-0.188
Entropy	0.031	-0.205	-0.245	-0.237

Table 8 : image 5445, correlation values occurrence texture, only damaged blocks

	21x21 (3;3)	21x21 (11;11)	51x51(21;21)
Mean	0.603	0.603	0.600
Variance	0.740	0.740	0.699
Homogeneity	-0.592	-0.578	-0.558
Contrast	0.743	0.713	0.679
Dissimilarity	0.722	0.693	0.665
Entropy	0.570	0.553	0.557
Second Moment	-0.389	-0.442	-0.429
Correlation	0.484	0.482	0.424

Table 9 : image 5445, correlation values co-occurrence texture, only damaged blocks

	7x7	13x13	17x17	21x21
Data Range	0.124	0.148	0.159	0.168
Mean	0.025	0.019	0.017	0.015
Variance	0.338	0.337	0.337	0.336
Entropy	0.083	0.122	0.143	0.108

Table 10 : image 2451, correlation values occurrence texture, only damaged blocks

	21x21 (3;3)	21x21 (11;11)	51x51(21;21)
Mean	-0.279	-0.279	-0.271
Variance	-0.238	-0.238	-0.246
Homogeneity	0.190	0.229	0.265
Contrast	-0.235	-0.270	-0.276
Dissimilarity	-0.204	-0.244	-0.251
Entropy	-0.158	-0.138	-0.168
Second Moment	0.134	0.156	0.199
Correlation	0.353	0.323	0.165

Table 11 : image 2451, correlation values co-occurrence texture, only damaged blocks

	7x7	13x13	17x17	21x21
Data Range	0.056	0.068	0.067	0.070
Mean	-0.031	-0.040	-0.051	-0.061
Variance	0.332	0.328	0.320	0.313
Entropy	-0.519	-0.496	-0.399	-0.372

Table 12 : image 2450, correlation values occurrence texture, only damaged blocks

	21x21 (3;3)	21x21 (11;11)	51x51(21;21)
Mean	-0.254	-0.254	-0.248
Variance	-0.240	-0.240	-0.249
Homogeneity	0.176	0.194	0.218
Contrast	-0.242	-0.267	-0.269
Dissimilarity	-0.210	-0.241	-0.242
Entropy	-0.142	-0.122	-0.145
Second Moment	0.111	0.125	0.149
Correlation	0.315	0.289	0.118

Table 13 : image 2450, correlation values co-occurrence texture, only damaged blocks

As expected, the correlations for the post-event images are increased, but not sufficiently to be confident of a strong link between damage and texture measure.

Similar levels of correlation were found on the Guan Xian, P.R.C. test case [20], although with more complex texture measures, i.e. homogeneity on a 51×51 pixel window and dx=21,dy=21. The highest correlation, i.e. with variance, may be tentatively explained considering a stronger speckle connected with a wider presence of small reflectors due to the randomly shaped debris stacks.

The only exception is represented by the values obtained for the co-occurrence texture measures of the 5445 image, for which some correlation coefficients were reported well above 0.7. This image, which is also the nearest to the catastrophic event, dating back to the 7th of April, is the only one among the three post-earthquake to be acquired with an incidence angle of 19.07°. Therefore it may be acceptable to assume that this incidence angle gives better results for our purposes. As is possible to see, the best results were obtained from co-occurrence texture measures, this may also be due to the fact that for viewing the damage caused by an earthquake, a directional component is needed, characteristic of this type of textural measures. At this point, to determine whether this hypothesis is realistic or purely due to chance, the same correlation coefficients were computed on co-occurrence texture measures from a pre-event image with the same incidence angle. The results are presented in Table 12:

	21x21 (3;3)	21x21 (11;11)	51x51(21;21)
Mean	0.490	0.490	0.492
Variance	0.686	0.686	0.643
Homogeneity	-0.430	-0.449	-0.441
Contrast	0.690	0.651	0.631
Dissimilarity	0.658	0.628	0.610
Entropy	0.418	0.422	0.449
Second Moment	-0.312	-0.352	-0.320
Correlation	0.442	0.443	-0.281

Table 12 : image 5457, correlation values co-occurrence texture, only damaged blocks

The correlation values obtained appear to be systematically closer to zero than the results from the corresponding post-event image 5445, revealing the existence of a link between damage due to the earthquake and the trend of the textural measures.

The correlations found are still too weak for an operational use, yet they encourage us to further investigate the issue. In particular, joint evaluation of more than one texture might lead to a more reliable estimation of the damage level.

B. A fusion proposal

As mentioned in sect. III, correlations between damage level and selected texture measures are definitely higher if damaged blocks only are considered. This suggested us to draft a damage assessment procedure as outlined in **Errore. L'origine riferimento non è stata trovata.**, where rough visual interpretation is used to select blocks with reportedly damaged buildings over which the block-level damage assessment is to be performed exploiting the correlations reported. The advantage of such apparent duplication of damage assessment operations would be in cross-validation of independent sources of information with respect to damage mapping.

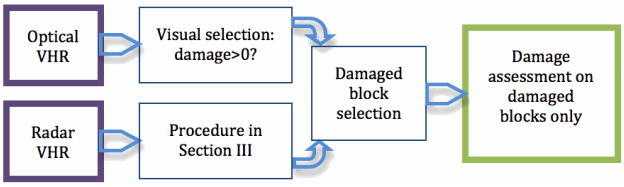

Figure 2: Fusion-based assessment procedure

IV. Conclusions

Investigations on earthquake damage assessment from post-event, very high resolution radar remotely sensed images have been presented. From our results it seems possible to conclude that basic statistical measures images can convey information on the damage level, although not all images are suitable for damage level assessment, and a large residual variability is still found, uncorrelated to actual damage level.

The damage assessment product is not to be considered operational yet, still the results encourage to move forward on its development. The most promising directions seem to be related with the joint exploitation of different statistics on the same image.

ACKNOWLEDGMENTS

This work has been partially funded by the Italian Department of Civil Protection through the "Piano Esecutivo 2009-2011" and by the European Commission through the SAFER Project. The authors wish to thank the people at the DPC and ASI for their efforts to deliver the data quickly. The work of Andrea Fenocchi in performing the experiments is also gratefully acknowledged.

REFERENCES

[1] S. Voigt, T. Kemper, T. Riedlinger, R. Kiefl, K. Scholte, and H. Mehl, "Satellite image analysis for disaster and crisis-management support, " IEEE Trans. Geosci. Remote Sens., vol. 45, no. 6, pp. 1520–1528,Jun. 2007.

[2] H. Aoki, M.Matsuoka, and F. Yamazaki, "Characteristics of satellite SAR images in the damaged areas due to the Hyogoken-Nanbu earthquake," in Proc. 19th Asian Conf. Remote Sens., 1998, vol. C7, pp. 1–6.

[3] M. Matsuoka and F. Yamazaki, "Use of satellite SAR intensity imagery for detecting building areas damaged due to earthquakes," Earthquake Spectra, vol. 20, no. 3, pp. 975–994, 2004.

[4] M. Matsuoka and F. Yamazaki, "Application of the damage detection method using SAR intensity images to recent earthquakes," in Proc. IGARSS, vol. 4, 2002, pp. 2042–2044.

[5] S. Stramondo, C. Bignami, M. Chini, N. Pierdicca, and A. Tertulliani, "The radar and optical remote sensing for damage detection: Results from different case studies," Int. J. Remote Sens., vol. 27, pp. 4433–4447, Oct. 20, 2006.

[6] C. Yonezawa and S. Takeuchi, "Decorrelation of SAR data by urban damage caused by the 1995 Hoyogoken-Nanbu earthquake," Int. J. Remote Sens., vol. 22, no. 8, pp. 1585–1600, 2001.

[7] Y. Ito, M. Hosokawa, H. Lee, and J. G. Liu, "Extraction of damaged regions using SAR data and neural networks," in Proc. 19th ISPRS Congr., Amsterdam, The Netherlands, Jul. 16–22, 2000, vol. 33, pp. 156–163.

[8] M. Chini, C. Bignami, S. Stramondo, and N. Pierdicca, "Uplift and subsidence due to the 26 December 2004 Indonesian earthquake detected by SAR data," Int. J. Remote Sens., vol. 29, no. 13, pp. 3891–3910, 2008.

[9] K. Saito, R. J. S. Spence, C. Going, and M. Markus, "Using high resolution satellite images for post-earthquake building damage assessment: A study following the 26 January 2001 Gujarat earthquake," Earthquake Spectra, vol. 20, no. 1, pp. 145–169, 2004.

[10] F. Yamakaki, M. Matsuoka, K. Kouchi, M. Kohiyama, and N. Muraoka, "Earthquake damage detection using high-resolution satellite images," in Proc. IGARSS, 2004, vol. 4, pp. 2280–2283.

[11] M. Matsuoka, T. T. Vu, and F. Yamazaki, “Automated damage detection and visualization of the 2003 Bam, Iran, earthquake using high resolution satellite images,” in Proc. 25th Asian Conf. Remote Sens., 2004, pp. 841–845.

[12] M. Chini, N. Pierdicca and W. J. Emery, “Exploiting SAR and VHR Optical Images to Quantify Damage Caused by the 2003 Bam Earthquake,” IEEE Trans. Geosci. Remote Sens., vol. 47, no. 1, pp. 145–152, Jan. 2009.

[13] F. Pacifici, F. Del Frate, C. Solimini, and W. J. Emery, “An innovative neural-net method to detect temporal changes in high-resolution optical satellite imagery,” IEEE Trans. Geosci. Remote Sens., vol. 45, no. 9, pp. 2940–2952, Sep. 2007.

[14] M. Chini, F. Pacifici, W. J. Emery, N. Pierdicca, and F. Del Frate, “Comparing statistical and neural network methods applied to very high resolution satellite images showing changes in man-made structures at Rocky Flats,” IEEE Trans. Geosci. Remote Sens., vol. 46, no. 6, pp. 1812–1821, Jun. 2008.

[15] J. Inglada and G. Mercier, “A new statistical similarity measure for change detection in multitemporal SAR images and its extension to multiscale change analysis,” IEEE Trans. Geosci. Remote Sens., vol. 45, no. 5, pp. 1432–1445, May 2007.

[16] Gamba, P.; Dell'Acqua, F.; Trianni, G., "Rapid Damage Detection in the Bam Area Using Multitemporal SAR and Exploiting Ancillary Data," IEEE Transactions on Geoscience and Remote Sensing, vol.45, no.6, pp.1582-1589, June 2007

[17] P. Gamba, F. Dell'Acqua, and G. Trianni, "Rapid Damage Detection in the Bam Area Using Multitemporal SAR and Exploiting Ancillary Data," IEEE Trans. Geosci. Remote Sens., vol.45, no.6, pp.1582-1589, June 2007.

[18] Y. Bazi, L. Bruzzone, and F. Melgani, “An unsupervised approach based on the generalized Gaussian model to automatic change detection in multitemporal SAR images,” IEEE Trans. Geosci. Remote Sens., vol.43, no.4, pp. 874-887, April 2005.

[19] F. Dell'Acqua, P. Gamba, L. Odasso, and G. Lisini, “Segment-based urban block outlining in high-resolution SAR images,” Urban Remote Sensing Event, 2009 Joint , CD-ROM Proc., pp.1-6, 20-22 May 2009.

[20] F. Dell’Acqua, G. Lisini, and P. Gamba, “Experiences in optical and SAR imagery analysis for damage assessment in the Wuhan, May 2008 earthquake,” Proc. of IGARSS 2009, Cape Town, South Africa, 13-17 July 2009.